Effects of β-hydroxybutyrate on restoring autophagic flux and mitochondrial function in macrophages exposed to oxidized low-density lipoprotein

WEIGUANG LUO[1*], MEI HE[2*] and HUILING WANG[1]

[1]Department of Clinical Laboratory, Henan Provincial People's Hospital, People's Hospital of Zhengzhou University, Zhengzhou, Henan 450003, P.R. China; [2]Henan Key Laboratory of Cardiac Remodeling and Transplantation, Zhengzhou No. 7 People's Hospital, Zhengzhou, Henan 450016, P.R China

Received February 5, 2026; Accepted May 6, 2026

DOI: 10.3892/mmr.2026.13943

Abstract. Atherosclerosis represents a major risk factor contributing to the development and advancement of cardiovascular diseases. The present study aimed to investigate the role of impaired autophagy and mitochondrial dysfunction in THP-1 macrophages induced by oxidized low-density lipoprotein (ox-LDL), a key factor in atherosclerosis and cardiovascular disease. The molecular mechanism underlying the contribution of ox-LDL to macrophage dysfunction is poorly understood. The present study aimed to determine whether β-hydroxybutyrate (BHB) protects autophagic and mitochondrial function in THP-1 macrophages exposed to ox-LDL. Using cell culture, western blotting, autophagy detection assay and measurement of mitochondrial membrane potential, the present study evaluated the effect of BHB on autophagic flux and mitochondrial integrity. Ox-LDL treatment markedly increased p62 protein levels and decreased LC3-II/LC3-I ratios, indicating impaired autophagy. BHB decreased p62 levels, increased LC3-II/LC3-I ratios and restored autophagic flux (shown by increased autophagosome numbers) and improved mitochondrial membrane potential. In addition, BHB downregulated STAT4, which was upregulated by ox-LDL, suggesting a signaling pathway through which BHB exerts its protective effect. The present findings demonstrate that BHB enhances autophagic activity and mitochondrial function in THP-1 macrophages under ox-LDL stress, highlighting its potential as a novel therapeutic agent for metabolic and cardiovascular disease. Future studies should examine *in vivo* applications and the broader implications of BHB in atherosclerosis.

Correspondence to: Dr Weiguang Luo or Dr Huiling Wang Department of Clinical Laboratory, Henan Provincial People's Hospital, People's Hospital of Zhengzhou University, 7 Weiwu Road, Zhengzhou, Henan 450003, P.R. China
E-mail: luo_weiguang@zzu.edu.cn
E-mail: mcolourful@126.com

*Contributed equally

Abbreviations: CVD, cardiovascular disease; ox-LDL, oxidized low-density lipoprotein; BHB: β-hydroxybutyrate; PMA, phorbol 12-myristate 13-acetate; SA-β-Gal, senescence-associated β-galactosidase; ROS, reactive oxygen species

Key words: β-hydroxybutyrate, autophagic flux, mitochondrial function, oxidized low-density lipoprotein, THP-1 cell

Introduction

Cardiovascular diseases (CVDs) are a leading cause of morbidity and mortality worldwide, accounting for an estimated 19.7 million deaths annually, representing ~32% of all global deaths (1). Among the risk factors for CVDs, oxidized low-density lipoprotein (ox-LDL) is a key driver of atherosclerosis, a disease characterized by the accumulation of fatty deposits in arterial walls (2,3). Previous studies have highlighted the detrimental effects of ox-LDL on macrophage function, especially its ability to promote inflammation and cell senescence (4,5). Moreover, the fact that ox-LDL contributes to atherosclerosis by inducing oxidative stress and inflammatory responses is well-established (6,7).

Autophagy is a key cellular process that degrades and recycles damaged organelles and proteins, thereby maintaining cell homeostasis (8). In macrophages, autophagy is particularly important because it regulates inflammation and lipid metabolism (9,10). Impaired autophagic activity is associated with pathophysiological conditions, including CVD and neurodegeneration (11). Macrophage autophagy promotes the catabolism of cytoplasmic lipid droplets, maintains cell lipid homeostasis and plays an important role in anti-atherosclerotic processes (12). Moreover, mitochondrial dysfunction, typically a consequence of oxidative stress, exacerbates these conditions (13). The interaction between autophagy and mitochondrial function is complex and understanding this interplay is essential for developing effective therapeutic interventions.

β-hydroxybutyrate (BHB), a ketone body generated during fatty acid metabolism, possesses anti-inflammatory properties and may protect cells from oxidative stress-induced damage (14). BHB also promotes autophagosome formation,

suggesting that it may be used therapeutically in metabolic disorders (15). The STAT signaling pathway is a critical component of cellular communication, primarily involved in regulating the transcription of target genes that are essential for cellular function (16). The clinical significance of the relationship between STAT signaling and autophagy is becoming increasingly evident (17,18). In cancer, for example, the activation of the JAK/STAT pathway leads to enhanced autophagic activity, which may contribute to tumor cell survival and resistance to therapy (19). Conversely, inhibiting the JAK/STAT pathway is associated with the promotion of autophagy and tumor cell death, indicating that targeting this signaling pathway could be a viable strategy for cancer treatment (20). The activation of the IL-12/STAT4 signaling pathway enhances autophagic activity, thereby contributing to the clearance of *Mycobacterium tuberculosis* in infected macrophages (21). Autophagy-related protein 5 can modulate immune responses by enhancing the production of CCL2, which influences STAT4 activation in $CD4^+$ T helper 1 cells during malaria infections (22). When macrophages are exposed to ox-LDL, STAT4 is phosphorylated and translocates to the nucleus, where it regulates the transcription of genes involved in inflammation (23). This leads to the production of pro-inflammatory cytokines such as IFN-γ and TNF-α, which are essential for the activation and recruitment of immune cells to the site of inflammation (24).

The molecular mechanisms by which BHB regulates autophagy and the role of STAT4 in this process remain incompletely understood. Further investigations are needed to delineate these pathways and assess their therapeutic relevance for autophagy-targeted interventions in lipid-related diseases. The present study aimed to examine the effects of BHB on autophagy and mitochondrial function in THP-1 macrophage exposed to ox-LDL and determine how BHB may restore cellular functions that are impaired by ox-LDL, with particular emphasis on the signaling molecule STAT4. The present findings could inform the development of novel therapeutic strategies for metabolic disorders and CVD.

Materials and methods

Reagents. (R)-(-)-β-Hydroxybutyric acid sodium salt (cat. no. 298360) was purchased from Sigma-Aldrich (Merck KGaA). ox-LDL (cat. no. YB-002) and 1,1'-dioctadecyl-3,3,3',3'-tetramethylindocarbocyanine perchlorate (Dil)-ox-LDL (cat. no. YB-0010) were obtained from Guangzhou Yiyuan Biotech Co., Ltd. Phorbol 12-myristate 13-acetate (PMA; cat. no. S1819) and the JC-1 Mitochondrial Membrane Potential (ΔΨm) Assay kit (cat. no. C2003S) were obtained from Beyotime Biotechnology. FBS (cat. no. 11011-8611) was purchased from Beijing Solarbio Science & Technology Co., Ltd. The Senescence-Associated β-Galactosidase (SA-β-Gal) Stain Kit (cat. no. G1580), BSA (cat. no. IA0910), Autophagy Staining Detection kit (cat. no. G0170), DAPI Staining Solution (cat. no. C0065), High-Efficiency RIPA Cell/Tissue Lysis Buffer (cat. no. R0010) and trypsin (cat. no. T1300) were obtained from Beijing Solarbio Science & Technology Co., Ltd. Rabbit anti-rat p62 (cat. no. ab109012), anti-STAT4 (cat. no. ab28815) and anti-β-actin antibody (cat. no. ab8226) were obtained from Abcam. ECL Plus Ultra-Sensitive Detection Reagent (cat. no. P0018AM), PVDF membrane (cat. no. FFP28), HRP-labeled goat anti-mouse IgG (cat. no. A0216) and HRP-labeled goat anti-rabbit IgG (cat. no. A0208) were obtained from Beyotime Biotechnology. The PAGE Gel Rapid Preparation kit (cat. no. PG112) was obtained from Epizyme Biotech. High-glucose DMEM (cat. no. SH30022.01) was purchased from Cytiva. Lipofectamine 2000 (cat. no. 11668030) and Opti-MEM reduced-serum medium (cat. no. 31985070) were purchased from Thermo Fisher Scientific, Inc.

Cell culture and treatment. THP-1 cells were purchased from GenChem Inc. and maintained in high-glucose DMEM supplemented with 10% FBS and 1% penicillin/streptomycin at 37˚C in a humidified atmosphere containing 5% CO_2. All experiments were performed using cells between passages 3 and 10 at ~80% confluency.

For macrophage differentiation, $2x10^5$ THP-1 cells per well were seeded in 6-well plates and stimulated with 100 ng/ml PMA at 37˚C for 24 h. Following PMA-induced monocyte-to-macrophage differentiation (confirmed by the transition to an adherent morphology), cells were washed twice with PBS. In the experiments involving both ox-LDL and BHB, the differentiated THP-1 macrophages were first incubated with 50 mg/l ox-LDL for 24 h at 37˚C, and then incubated with BHB (1, 2 or 3 mM) for 24 h at 37˚C.

Western blot analysis. A total of $2x10^5$ THP-1 cells per well seeded in 6-well plates were stimulated with 100 ng/ml PMA for 24 h at 37˚C. The differentiated THP-1 macrophages were treated with either ox-LDL or BHB for an additional 24 h at 37˚C. Cells were harvested and washed twice with ice-cold PBS. Protein extraction was performed using 100 µl high-efficiency RIPA lysis buffer supplemented with 1 µl PMSF by incubating on ice for 30 min. Lysates were centrifuged at 12,000 x g for 20 min at 4˚C, mixed with 25 µl 5X loading buffer, denatured at 100˚C for 10 min and immediately chilled on ice. Samples were stored at -20˚C until analysis.

Protein concentration was determined using the BCA assay. Equal amounts of protein (20 µg/lane) were separated on 10% SDS-polyacrylamide gels and transferred onto PVDF membranes at 100 V. Membranes were blocked with 5% BSA for 2 h at room temperature, followed by incubation with primary antibodies (1:1,000) overnight at 4˚C. HRP-conjugated goat anti-rabbit secondary antibody (1:5,000) or HRP-conjugated goat anti-mouse secondary antibody (1:5,000) was applied for 2 h at room temperature. Protein signals were detected using ECL reagents. Band intensities were quantified using ImageJ software (ImageJ 1.53t; National Institutes of Health) with β-actin as the loading control.

Autophagy detection. A total of $4x10^4$ THP-1 cells per well were seeded onto sterile glass coverslips placed in 24-well plates. Following stimulation with 100 ng/ml PMA at 37˚C for 24 h, cells were washed twice with PBS. THP-1 cells in different experimental groups were treated as follows: In the experiment to determine the optimal concentration of ox-LDL, differentiated THP-1 macrophages were incubated with ox-LDL (0, 50 and 100 mg/l) at 37˚C for 24 h; in experiments involving ox-LDL and BHB, differentiated THP-1

macrophages were first incubated with 50 mg/l ox-LDL at 37˚C for 24 h, and then incubated with BHB (1, 2 or 3 mM) at 37˚C for 24 h; and in experiments involving overexpression and inhibition of STAT4, after the overexpression and inhibition of STAT4, 50 mg/l ox-LDL was added (or not added) and cells were incubated at 37˚C for 24 h, followed by the addition (or non-addition) of 3 mM BHB and incubation at 37˚C for 24 h.

After the aforementioned treatment, the cells were processed with an Autophagy Staining Detection kit, according to the manufacturer's protocol. Briefly, cells were gently rinsed twice with wash buffer, then incubated with dansylcadaverine for 15-30 min at room temperature under light-protected conditions. Following two additional washes, nuclei were counterstained with DAPI (1 μg/ml) for 5-10 min at 25˚C. Following final rinsing with wash buffer, the coverslips were mounted onto adhesive microscope slides using an anti-fade mounting medium (cat. no. S2100; Beijing Solarbio Science & Technology Co., Ltd.).

Autophagic vesicles were visualized with a laser-scanning confocal microscope (FV3000; Olympus Corporation). Excitation/emission settings were set to optimal dye parameters (488 nm excitation/530 nm emission) and for DAPI (405 nm excitation/461 nm emission). Images were acquired using sequential channel scanning to avoid fluorescence bleed-through.

ΔΨm assessment. A total of 4x10^4 THP-1 cells per well grown on glass coverslips in 24-well plates. Following stimulation with 100 ng/ml PMA at 37˚C for 24 h, cells were washed twice with PBS. Cell treatments and grouping were the same as described in the autophagy detection section.

After the aforementioned treatment, the cells were processed with the JC-1 Mitochondrial Membrane Potential (ΔΨm) Assay kit (cat. no. C2003S; Beyotime Biotechnology) according to the manufacturer's protocol. Briefly, a JC-1 dye working solution was prepared by diluting the stock solution 1:1 in complete culture medium (high-glucose DMEM supplemented with 10% FBS and 1% penicillin/streptomycin). The cells were incubated with this mixture for 20 min at 37˚C under light-protected conditions. After incubation, the coverslips were washed twice with JC-1 assay buffer, transferred to fresh culture medium and mounted face-down onto adhesive microscope slides using an anti-fade mounting medium. The ΔΨm assessment was performed by observing the aggregated (red) or monomeric (green) state of JC-1 in the cells with a laser-scanning confocal microscope (FV3000; Olympus Corporation). Fluorescence intensities were quantified using ImageJ software (ImageJ 1.53t; National Institutes of Health).

Senescence-associated β-Gal (SA-β-Gal) staining. A total of 4x10^4 THP-1 cells per well were seeded in 24-well plates. Following stimulation with 100 ng/ml PMA at 37˚C for 24 h, cells were washed twice with PBS. Differentiated THP-1 macrophages were first incubated with 50 mg/l ox-LDL at 37˚C for 24 h, and then incubated with BHB (0,1, 2 or 3 mM) at 37˚C for 24 h. After the aforementioned treatment, the cells were washed twice with PBS and fixed with 4% formaldehyde for 15 min at room temperature. Following three PBS washes, the cells were incubated with 1 ml β-Gal staining solution [1 mg/ml X-Gal, 5 mM potassium ferrocyanide, 5 mM potassium ferricyanide, 150 mM NaCl, 2 mM $MgCl_2$ in 40 mM citric-acid/sodium-phosphate buffer (pH 6.0)] under an airtight seal with paraffin film at 37˚C in a non-CO_2 atmosphere for 24 h. After two additional PBS washes, SA-β-Gal-positive cells (blue staining) were examined under a fluorescence microscope. Semi-quantitative analysis of fluorescence intensity was performed using ImageJ software (version 1.54f; National Institutes of Health). In total, five random fields of view/well were imaged for statistical analysis.

Fluorescent ox-LDL uptake assay. A total of 4x10^4 THP-1 cells per well were seeded in 24-well plates and differentiated with 100 ng/ml PMA for 24 h at 37˚C. The resulting macrophages were incubated with 100 μg/ml DiI-ox-LDL together with BHB (0, 1, 2, 3 mM) for 24 h at 37˚C, 5 % CO_2. After incubation, the cells were washed three times with PBS. Fluorescent micrographs were captured with an inverted fluorescence microscope. Intracellular DiI-ox-LDL accumulation was quantified with ImageJ software (version no. 1.53t, National Institutes of Health), by analyzing fluorescence intensity in three independent biological replicates.

Total RNA extraction and reverse transcription-quantitative PCR (RT-qPCR). Total RNA was isolated from THP-1 cells using an RNA isolation kit (cat. no. R0026; Beyotime Biotechnology) according to the manufacturer's instructions. Briefly, after adding the lysis buffer to the THP-1 cell culture plate, the cells were lysed and incubated at room temperature for 5 min. Subsequently, 200 μl chloroform was added, and the mixture was vigorously shaken for 15 sec, followed by incubation at room temperature for 3 min. The sample was then centrifuged at 13,000 x g for 10 min at 4˚C. The supernatant was transferred to a new tube. An equal volume of ethanol was slowly added, followed by thorough mixing. The solution along with any precipitate was transferred into an adsorption column (CR3) and centrifuged at 13,000 x g for 30 sec at 4˚C. Subsequently, 500 μl protein removal solution was added, followed by centrifugation at 13,000 x g for 30 sec at 4˚C, and the flow-through was discarded. The CR3 column was placed into a collection tube, and 500 μl wash buffer was added. After incubation at room temperature for 2 min, the column was centrifuged at 13,000 x g for 30 sec at 4˚C, and the flow-through was discarded. The column was transferred to a 2 ml collection tube and centrifuged at 13,000 x g for 2 min at 4˚C to remove residual liquid. Finally, the CR3 column was placed into a new 1.5-ml microcentrifuge tube, and 40 μl RNase-free ddH_2O was added. After incubation at room temperature for 2 min, the tube was centrifuged at 13,000 x g for 2 min at 4˚C. The extracted RNA was used for subsequent experiments.

Reverse transcription was performed using an RT-PCR kit (cat. no. RP1100; Beijing Solarbio Science & Technology Co., Ltd.). Briefly, in a total reaction volume of 14.5 μl, 2 μg of RNA and 2 μl of the specific primer Oligo$(dT)_{16}$ were added, and the volume was adjusted with RNase-free ddH_2O. The mixture was incubated at 70˚C for 5 min and then rapidly cooled on ice for 2 min. After a brief centrifugation at 500 x g for 30 sec at 4˚C to collect the reaction mixture, the following components were added: 4 μl 5X M-MLV Buffer, 1 μl dNTPs, 0.5 μl

RNasin and 1 μl M-MLV reverse transcriptase. The reaction was incubated at 42˚C for 60 min, followed by heating at 95˚C for 5 min to terminate the reaction. The product was placed on ice for subsequent experiments.

qPCR was performed using 2X SYBRGreen PCR Mastermix (cat. no. SR1110; Beijing Solarbio Science & Technology Co., Ltd.). Briefly, the following components were added to a reaction tube: 12.5 μl of 2X SYBR Green PCR mix, 1 μl of primers (10 μM), 5 μl of template DNA and 5.5 μl of ddH_2O, to a final volume of 25 μl. The reaction was performed using an Applied Biosystems StepOnePlus real-time PCR system (Thermo Fisher Scientific, Inc.) under the following conditions: Initial denaturation at 95˚C for 3 min; 40 cycles of denaturation at 95˚C for 20 sec, annealing at 60˚C for 25 sec and extension at 72˚C for 30 sec (with fluorescence acquisition during the extension step). The cycle threshold (Ct) value was analyzed using StepOne software v2.3 (Thermo Fisher Scientific, Inc.), semilog amplification curves were evaluated using the comparative quantification method ($2^{-\Delta\Delta Cq}$) (25) and the gene expression levels were normalized to those of human β-actin. The primer pairs for qPCR were: STAT4 forward, 5'-CCTGACATTCCCAAAGACAAAGC-3' and reverse, 5'-TCTCTCAACACCGCATACACAC-3'; and β-actin forward, 5'-GTGGACATCCGCAAAGAC-3' and reverse, 5'-AAAGGGTGTAACGCAACTA-3'.

STAT4 overexpression via Lipofectamine-mediated transfection. The PCDNA3.1-STAT4 (*Homo sapiens*, XM_054343566.1) expression plasmid was purchased from BGI Genomics and the empty PCDNA3.1 vector (BGI Genomics) was also transfected as a negative control. A total of $2x10^5$ THP-1 cells per well were seeded in 6-well plates at ~80 % confluency and differentiated with 100 ng/ml PMA for 24 h at 37˚C. The medium was replaced with antibiotic-free complete DMEM (Cytiva). Lipofectamine 2000 (10 μl) was diluted in 250 μl Opti-MEM® I Reduced-Serum Medium. Plasmid DNA (5 μg) was diluted in 250 μl Opti-MEM. Following a 5 min incubation at room temperature, the diluted DNA and Lipofectamine solutions were combined, vortexed gently and incubated for 15 min at room temperature. The resulting DNA-lipid complexes were added dropwise to the cells. Following 6 h of incubation at 37˚C with 5 % CO_2, the transfection medium was replaced with fresh complete DMEM (Cytiva). The expression of STAT4 was validated by RT-qPCR. RT-qPCR was used to verify the overexpression efficiency of STAT4 before treating cells with ox-LDL or BHB. THP-1 cells were seeded into 6-well plates at a density of $2x10^5$ cells per well and stimulated with 100 ng/ml PMA at 37˚C for 24 h. Following transfection according to the aforementioned procedure, the cells were collected for total RNA extraction. Subsequently, RT-qPCR was conducted to detect STAT4 mRNA levels in order to confirm the transfection efficiency.

STAT4 silencing. The STAT4 gene-silencing kit (genOFF h-STAT4_2500A) was used according to the manufacturer's protocol (cat. no. SIGS0000957-4; Guangzhou RiboBio Co., Ltd.). The STAT4 siRNA target sequence was 5'-GCCTGA CCATAGATTTGGA-3' (the corresponding siRNA was provided by Guangzhou RiboBio Co., Ltd.), and the negative control siRNA (cat. no. SIGS0000957-4; Guangzhou RiboBio Co., Ltd.) was provided by Guangzhou RiboBio Co., Ltd. A total of $2x10^5$ THP-1 cells per well were seeded in 6-well plates. Following 24 h of stimulation with 100 ng/ml PMA at 37˚C, the medium was replaced with antibiotic-free complete DMEM. The Ribo FECT™ CP buffer was diluted with PBS and the STAT4 siRNA and the negative control siRNA included in the STAT4 gene-silencing kit were briefly centrifuged (500 x g; 1 min) at 25˚C, resuspended in 250 μl sterile de-ionized water, aliquoted and stored at -20˚C. For the transfection mixture, 120 μl diluted Ribo FECT CP buffer, 10 μl 50 nM STAT4 siRNA and 12 μl Ribo FECT CP reagent were incubated at room temperature for 15 min and then added dropwise to the 6-well plates. Following 48 h of incubation at 37˚C with 5% CO_2, the expression of STAT4 was validated by RT-qPCR. RT-qPCR was used to verify the silencing efficiency of STAT4 before treating cells with ox-LDL or BHB. THP-1 cells were seeded into 6-well plates at a density of $2x10^5$ cells per well and stimulated with 100 ng/ml PMA at 37˚C for 24 h. Following transfection according to the aforementioned procedure, the cells were collected for total RNA extraction. Subsequently, RT-qPCR was conducted as aforementioned to detect STAT4 mRNA levels in order to confirm the transfection efficiency.

Statistical analysis. Data were analyzed using GraphPad Prism® software (version 10.1.2; GraphPad Software, Inc.; Dotmatics). All experiments were independently repeated at least three times. All data are presented as the mean ± SEM. Statistical analysis was performed using one-way ANOVA followed by Bonferroni's post hoc test. $P<0.05$ was considered to indicate a statistically significant difference.

Results

ox-LDL induces impaired autophagic flux and decreased ΔΨm in THP-1 cells. The present study assessed the expression of p62, a selective substrate for autophagic degradation, in THP-1 cells following ox-LDL stimulation. Immunoblot analysis revealed that ox-LDL (50 and 100 mg/l) significantly increased p62 expression and decreased the ratio of LC3-II/LC3-I compared with untreated controls (Fig. 1A-C). To corroborate these findings, autophagosome formation was evaluated using confocal laser scanning microscopy. Cells treated with ox-LDL (100 mg/l) exhibited a marked reduction in autophagic puncta, consistent with the immunoblot data, indicating impaired autophagy (Fig. 1D and F). ΔΨm was measured using the JC-1 fluorescent probe. Red fluorescence, indicating high ΔΨm, was observed in control cells. By contrast, ox-LDL treatment (100 mg/l) led to significantly attenuated red fluorescence intensity and a concomitant increase in green fluorescence (indicating a reduction in ΔΨm; Fig. 1E and G). These results demonstrate that ox-LDL exposure induces a substantial decrease in ΔΨm in THP-1 cells. Collectively, these findings indicated mitochondrial dysfunction, reflecting a diminished capacity to maintain cell energy metabolism and homeostasis.

BHB restores impaired autophagic flux and ΔΨm in ox-LDL-treated THP-1 cells. The present study assessed the effect of BHB on autophagic flux in THP-1 cells. p62 expression levels decreased significantly, while ratio of LC3-II/LC3-I

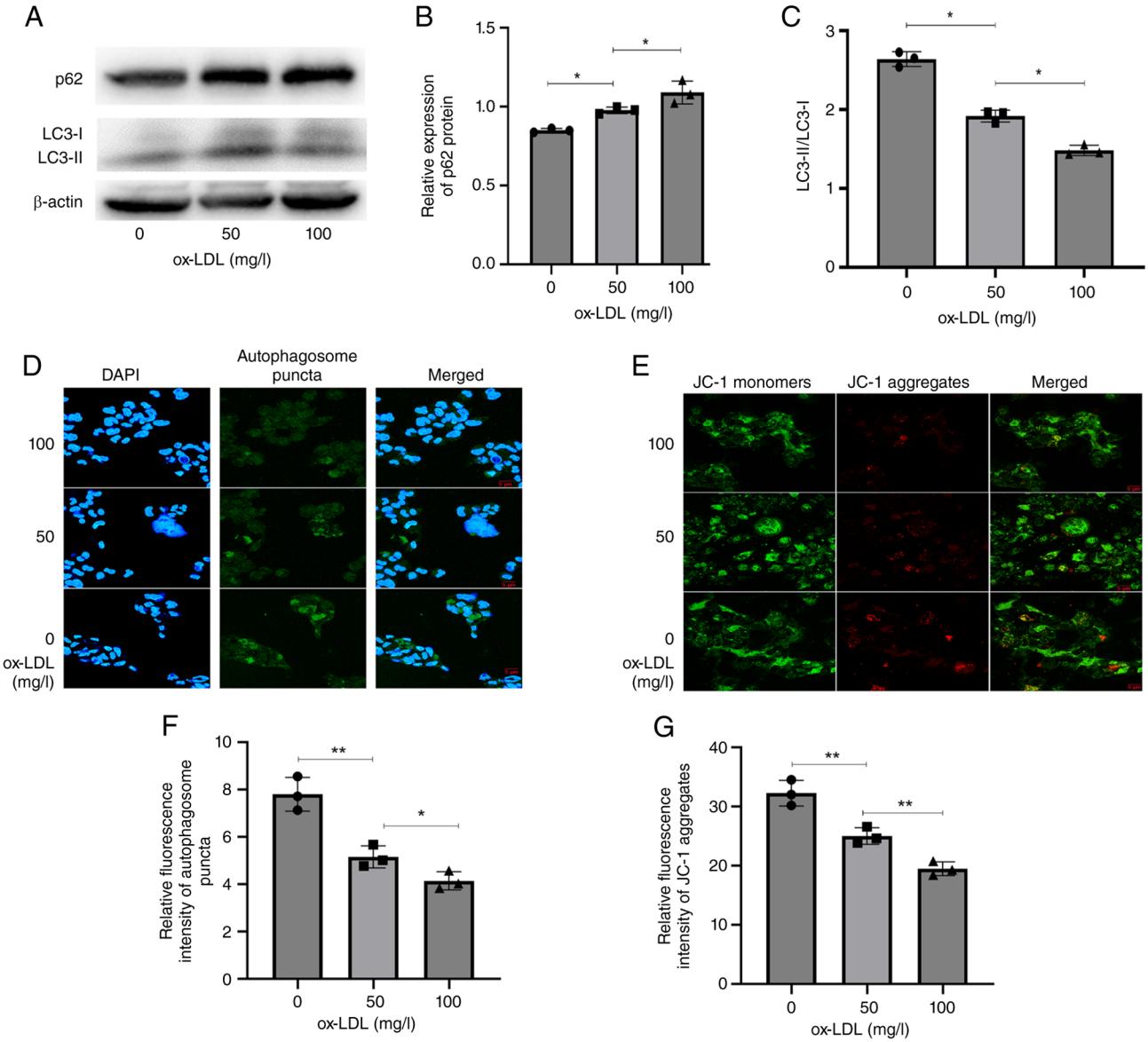

Figure 1. ox-LDL impairs autophagic flux and reduces the mitochondrial membrane potential. (A) Western blot analysis of (B) p62 and LC3 in THP-1 cells treated with ox-LDL at various doses for 24 h. (C) Quantification of LC3II/LC3-I ratios. (D) Confocal microscopy image of autophagosome puncta in ox-LDL-treated cells stained with dansylcadaverine. Nuclei were visualized by counterstaining with DAPI (magnification, x60). (E) JC-1 staining of THP-1 cells. Fluorescence was recorded using 488 nm excitation (magnification, x60). Relative fluorescence intensity of (F) autophagosome puncta and (G) JC-1 aggregates. *P<0.05, **P<0.01. ox-LDL, oxidized low-density lipoprotein.

increased markedly following BHB treatment, indicating that BHB effectively restored the impaired autophagic flux in THP-1 cells (Fig. 2A-C). Cells treated with both ox-LDL and BHB at 1 and 2 mM exhibited a higher expression of p62 compared with those exposed solely to ox-LDL, while a notable decrease in expression was observed at 3 mM BHB. Fluorescent staining confirmed this restoration: While 1 mM and 2 mM BHB reduced autophagic puncta formation and ΔΨm, 3 mM BHB markedly increased both autophagic puncta (Fig. 2D and F) and ΔΨm (Fig. 2E and G). Collectively, these results demonstrate that BHB enhances autophagic capacity and mitochondrial function in THP-1 macrophages by ameliorating ox-LDL-induced impairment of autophagic flux.

BHB decrease ox-LDL accumulation and β-Gal activity in THP-1 cells. BHB co-treatment significantly decreased Dil-ox-LDL levels in THP-1 cells, indicating potent inhibition of ox-LDL accumulation in macrophages (Fig. 3A and B). As elevated β-Gal activity serves as a key marker of cell senescence (26), this was measured following 24 h of co-treatment with ox-LDL and BHB. BHB suppressed intracellular β-Gal activity in a dose-dependent manner (Fig. 3C and D), suggesting attenuation of cell aging processes.

BHB downregulates STAT4 expression in ox-LDL-treated THP-1 cells. ox-LDL significantly upregulated STAT4 protein expression in THP-1 cells (Fig. 4A and B). Conversely, BHB substantially decreased STAT4 levels in a dose-dependent manner.

STAT4 overexpression impairs BHB-mediated restoration of autophagic flux. The present study examined the role of STAT4

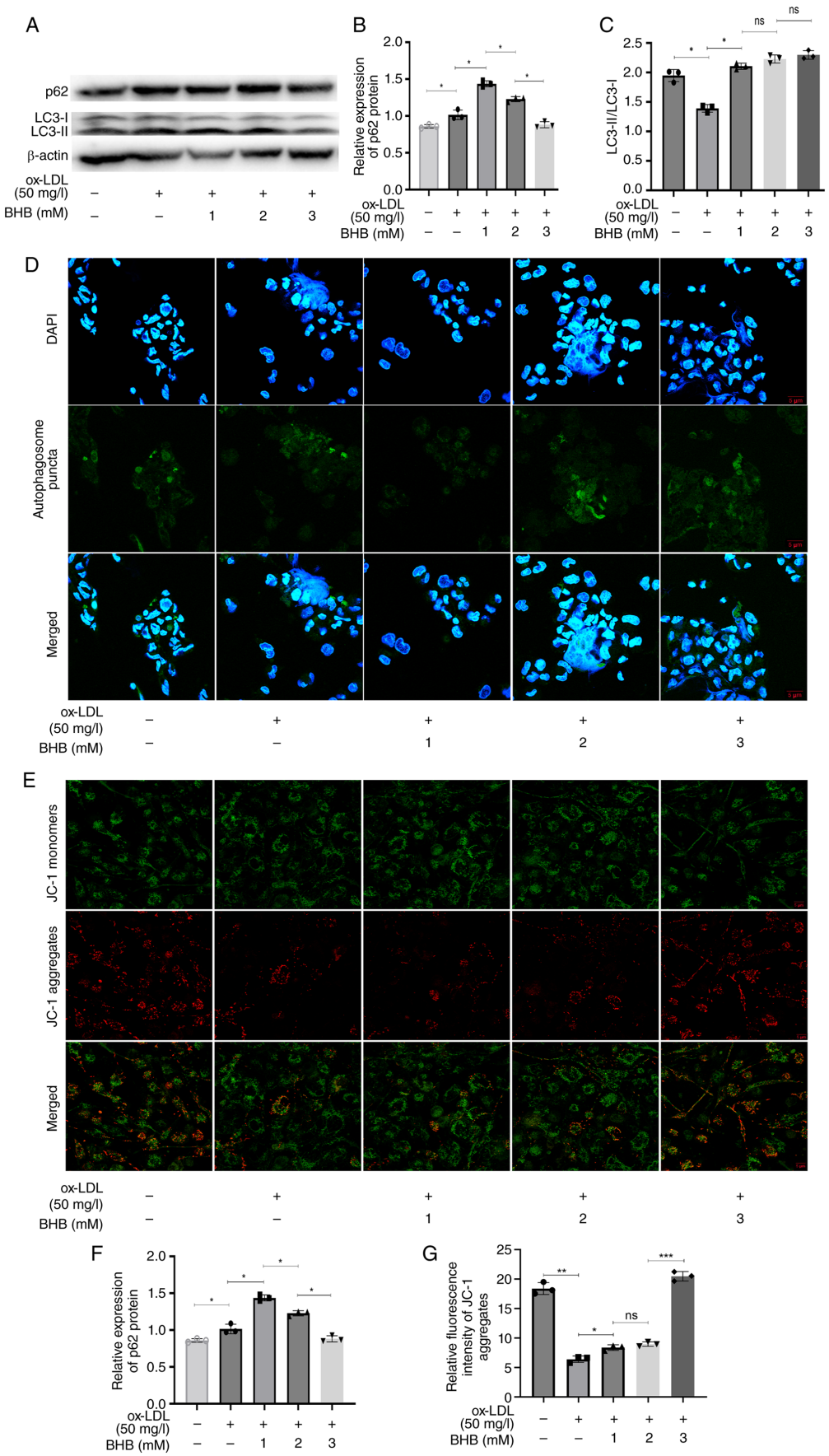

Figure 2. BHB restores impaired autophagic flux and mitochondrial membrane potential. (A) Western blot analysis of (B) p62 and LC3 in THP-1 cells treated with ox-LDL and BHB for 24 h. (C) LC3II/LC3-I ratios. (D) Confocal microscopy image of autophagosome puncta in cells treated with ox-LDL and BHB. Nuclei were counterstained with DAPI (magnification, x60). (E) JC-1 staining of THP-1 cells visualized by fluorescence confocal microscopy. Fluorescence was recorded using 488 nm excitation (magnification, x60). Relative fluorescence intensity of (F) autophagosome puncta and (G) JC-1 aggregates in cells treated with ox-LDL and BHB. *P<0.05, **P<0.01, ***P<0.001. ox-LDL, oxidized low-density lipoprotein; BHB, β-hydroxybutyrate; ns, not significant.

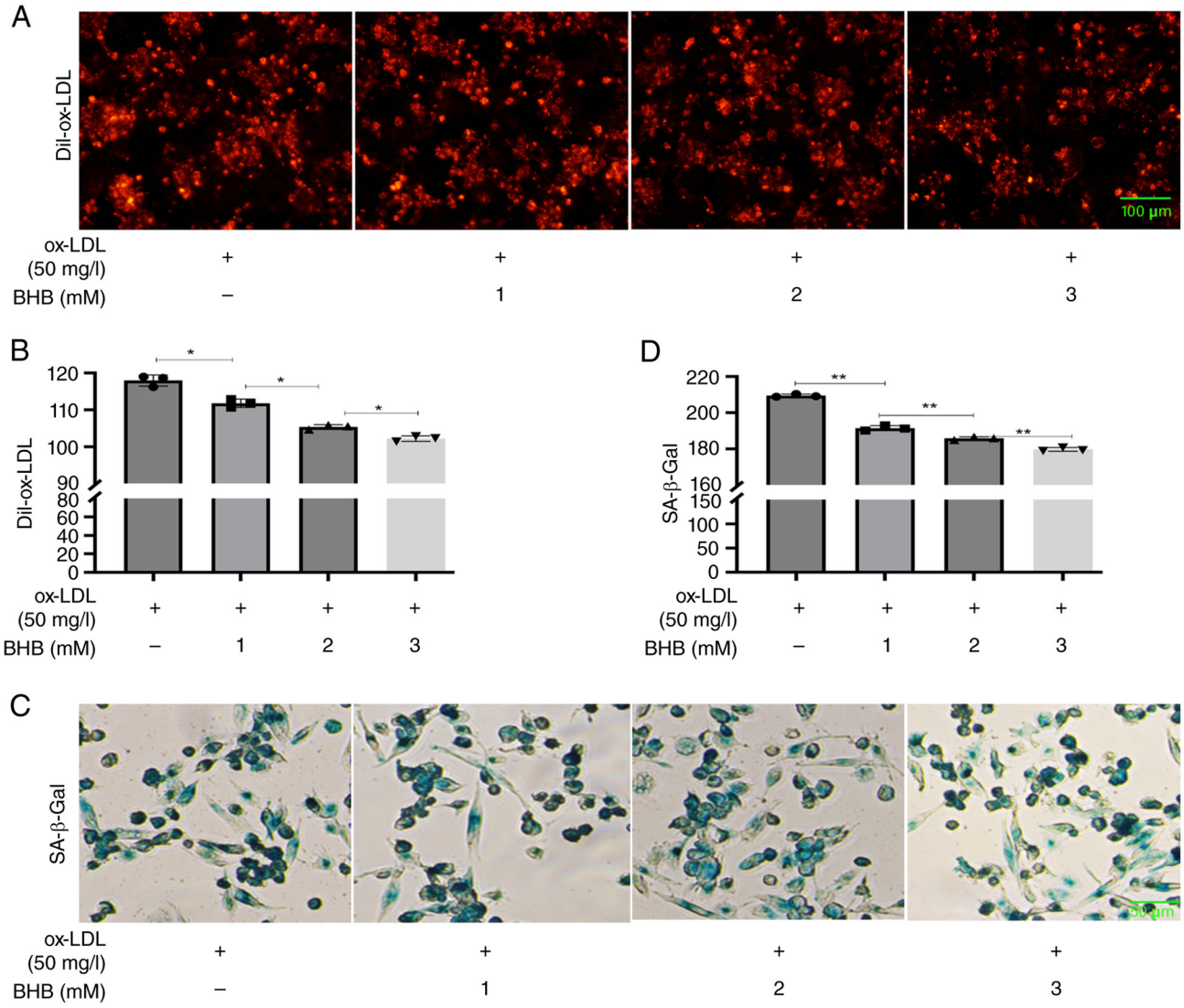

Figure 3. BHB decreases ox-LDL accumulation and β-Gal activity. (A) Representative fluorescence microscopy of (B) Dil-ox-LDL uptake in THP-1 cells. Scale bar, 100 μm. (C) Representative (D) SA-β-Gal staining. Scale bar, 50 μm. *P<0.05, **P<0.01. BHB, β-hydroxybutyrate; Dil-ox-LDL, 1,1'-dioctadecyl-3,3,3',3'-tetramethylindocarbocyanine perchlorate-oxidized low-density lipoprotein; SA-β-Gal, senescence-associated β-galactosidase.

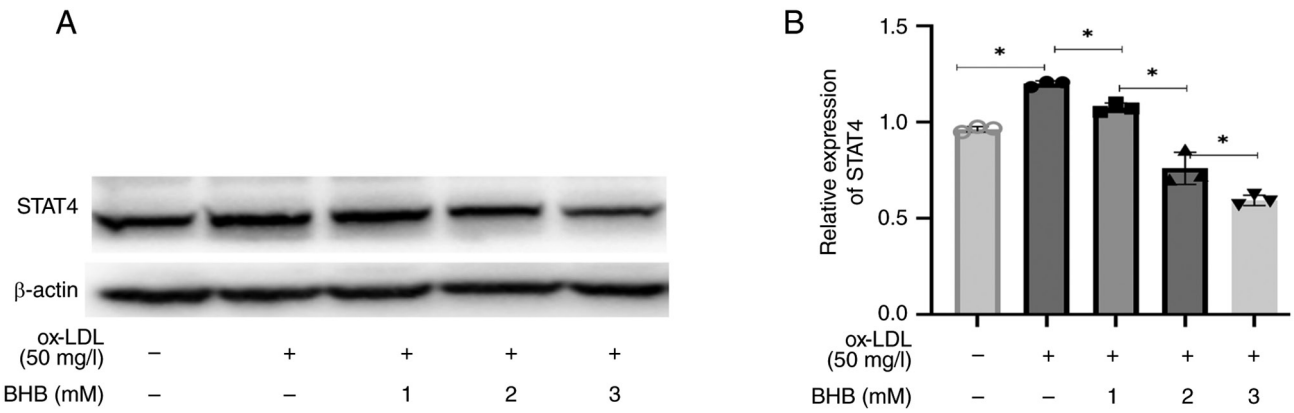

Figure 4. BHB downregulates STAT4 expression in ox-LDL-treated THP-1 cells. (A) Western blot analysis of (B) STAT4 expression in THP-1 cells treated with ox-LDL and BHB. *P<0.05. BHB, β-hydroxybutyrate; ox-LDL, oxidized low-density lipoprotein.

in mediating the rescue effect of BHB on ox-LDL-induced impairment of autophagic flux. Following overexpression of STAT4 (Fig. S1A), p62 levels increased significantly (Fig. 5A-C), whereas autophagic puncta decreased (Fig. 5D and F) and the

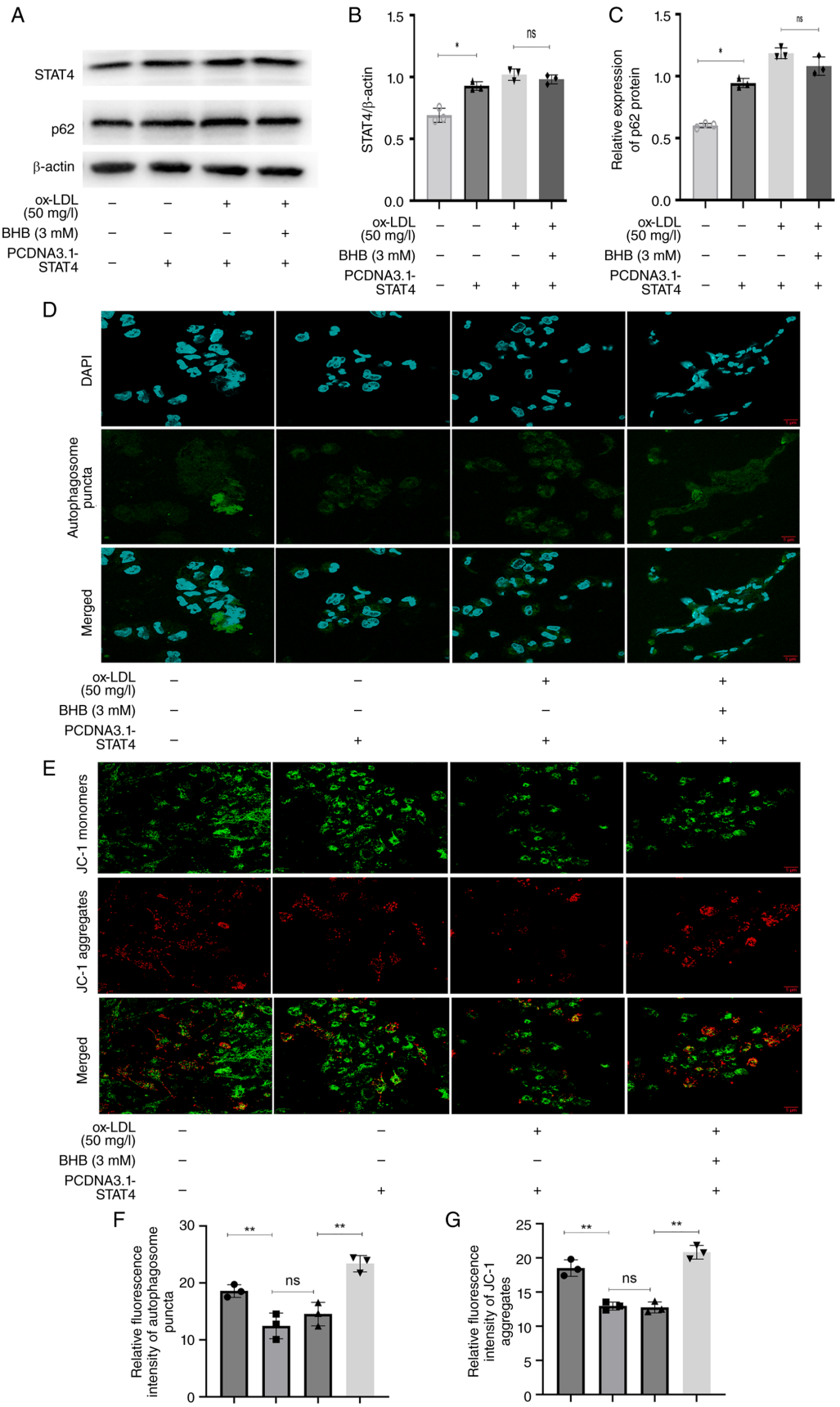

Figure 5. STAT4 overexpression impairs the ability of BHB to restore autophagic flux. (A) Western blot analysis of (B) STAT4 and (C) p62 in STAT4-overexpressing THP-1 cells treated with ox-LDL and BHB. (D) Confocal microscopy image of autophagosome puncta in STAT4-overexpressing THP-1 cells following ox-LDL and BHB treatment. Nuclei were visualized by counterstaining with DAPI (magnification, x60). (E) JC-1 staining of THP-1 cells imaged by fluorescence confocal microscopy. Fluorescence was recorded using 488 nm excitation (magnification, x60). Relative fluorescence intensity of (F) autophagosome puncta and (G) JC-1 aggregates in STAT4-overexpressing THP-1 cells after ox-LDL and BHB treatment. The group without 50 mg/l ox-LDL, 3 mM BHB and PCDNA3.1-STAT4 treatment was transfected with the empty vector. *P<0.05, **P<0.01. BHB, β-hydroxybutyrate; ox-LDL, oxidized low-density lipoprotein; ns, not significant.

ΔΨm declined (Fig. 5E and G). Following co-treatment with ox-LDL and BHB, STAT4-overexpressing cells exhibited no significant alterations in p62 expression, autophagosome count or ΔΨm. Collectively, these findings demonstrate that STAT4 overexpression abrogated BHB-mediated restoration of impaired autophagic flux and mitochondrial function.

STAT4 silencing prevents Ox-LDL-induced impairment of autophagic flux and Ox-LDL-induced reduction of the ΔΨm in THP-1 cells. siRNA transfection was performed to explore the role of STAT4 in autophagic recovery and ox-LDL uptake. Compared with cells transfected with scrambled RNA (Fig. S1B), STAT4 silencing significantly decreased p62 expression (Fig. 6A-C), increased autophagosome formation (Fig. 6D and F) and elevated ΔΨm (Fig. 6E and G). However, when ox-LDL was added following siRNA-STAT4 transfection in THP-1 cells, the results did not show the same pattern as before in non-siRNA-STAT4-transfected THP-1 cells [increased p62 expression levels, impaired autophagic flux (Fig. 1A-F) and decreased ΔΨm (Fig. 1E and G)]. As aforementioned, silencing of STAT4 markedly attenuated ox-LDL-induced impairment of autophagic flux and the accompanying decline in ΔΨm in THP-1 cells.

Discussion

The pathophysiology of CVD, particularly atherosclerosis, is influenced by the accumulation of ox-LDL, which serves a pivotal role in macrophage dysfunction and foam cell formation (27). This accumulation initiates a cascade of inflammatory responses and promotes cell senescence, contributing to disease progression and enhancing susceptibility to other types of metabolic disorder, such as glucose metabolism disorders (28,29).

The present study examined the impact of BHB on autophagy and mitochondrial function in THP-1 macrophages exposed to ox-LDL. ox-LDL impairs autophagic flux and compromises mitochondrial integrity, resulting in elevated cell stress and inflammation (30). Here, BHB significantly restored autophagic function and enhanced ΔΨm in these cells, implying a potential therapeutic benefit of BHB in mitigating the deleterious effects of ox-LDL. Moreover, modulation of the STAT4 signaling pathway is a key mechanism by which BHB exerts its restorative effects, underscoring the importance of targeting autophagy to improve macrophage function in atherosclerosis (31).

Recent studies have demonstrated that ox-LDL-induced impairment of autophagy flux and mitochondrial dysfunction in THP-1 macrophages serve critical roles in the progression of atherosclerosis (32,33). Gu *et al* (34) showed that ox-LDL impairs autophagy flux in THP-1 cells, whereas treatment with nicotinate-curcumin rescues the impaired autophagic flux by significantly increasing LC3-II levels, autolysosome numbers and p62 degradation in ox-LDL-treated THP-1 cells, similar to the present study. The present study examined the expression of the key selective autophagy protein p62. Accumulation of p62 protein typically suggests impairment or inhibition of autophagic flux (35). Changes in p62 alongside LC3-II levels reflect autophagic activity (36). The present study demonstrated an increase in LC3-II levels along with a decrease in p62, indicating overall activation of autophagic flux (37,38).

In human umbilical vein endothelial cells (HUVECs) treated with ox-LDL, silencing of syntaxin 17, a key regulator of autophagosome-lysosome fusion, exacerbates autophagic flux impairment and inflammatory responses (39). Here, ox-LDL induced decreased ΔΨm in THP-1 macrophages, a phenomenon increasingly associated with oxidative stress and inflammatory signaling (40,41). Erianin reverses ox-LDL-induced decreased ΔΨm in HUVECs by activating the Nrf2 pathway, which enhances antioxidant defenses (42). These findings align with the present observations, suggesting that decreased ΔΨm may stem from impaired electron transport chain activity and ROS accumulation.

BHB, a primary ketone body, serves a key role in regulating macrophage function and foam cell formation. A recent study has demonstrated that BHB suppresses pro-inflammatory M1 macrophage polarization by inducing histone β-hydroxybutyrylation (Kbhb) of STAT1 at lysine 679, thereby inhibiting its phosphorylation and inflammatory cytokine production (such as IL-1β and TNF-α) (43). Conversely, BHB promotes anti-inflammatory M2 polarization via STAT6-dependent pathways, enhancing the secretion of IL-10 and arginase-1 (Arg-1), which facilitates tissue repair and decreases lipid accumulation in macrophages (44). In atherosclerosis models, BHB decreases ox-LDL uptake by downregulating scavenger receptors (such as CD36) and upregulating cholesterol efflux transporters (ATP-binding cassette protein A1 and ATP-binding cassette transporter G1), thereby attenuating foam cell formation (45,46). These immunometabolic shifts underscore the dual role of BGB in mitigating inflammation and lipid overload, positioning it as a promising therapeutic candidate for vascular pathology.

BHB directly modulates STAT transcription factors through epigenetic and post-translational mechanisms (47). Bai *et al* (43) identified that BHB induces Kbhb modification of STAT1 at lysine 679, which impairs its phosphorylation and nuclear translocation, thereby inhibiting lipopolysaccharide-driven M1 polarization. Conversely, BHB activates STAT6 phosphorylation via IL-4 receptor α signaling, driving M2-associated gene expression. In endothelial cells, BHB enhances STAT6-mediated Nrf2 activation, thereby boosting antioxidant defenses and decreasing oxidative stress (48). This STAT-centric regulation underpins the ability of BHB to rebalance macrophage phenotypes by suppressing STAT1/NF-κB-driven inflammation and amplifying STAT6-mediated resolution pathways. These mechanisms may contribute to the decreased plaque instability observed in atherosclerotic models treated with BHB or ketogenic diets (49,50).

STAT signaling intersects with mitochondrial homeostasis and autophagy, which are key for macrophage lipid metabolism (51). STAT1 hyperactivation promotes mitochondrial ROS overproduction and membrane depolarization, thereby exacerbating oxidative damage and impairing mitophagy (52). By contrast, STAT6 activation by BHB upregulates Nrf2, which enhances mitochondrial biogenesis and stabilizes membrane potential via peroxisome proliferator-activated receptor γ coactivator 1-α (48,53). Furthermore, STAT6-dependent induction of Arg-1 supports autophagy flux through mTOR

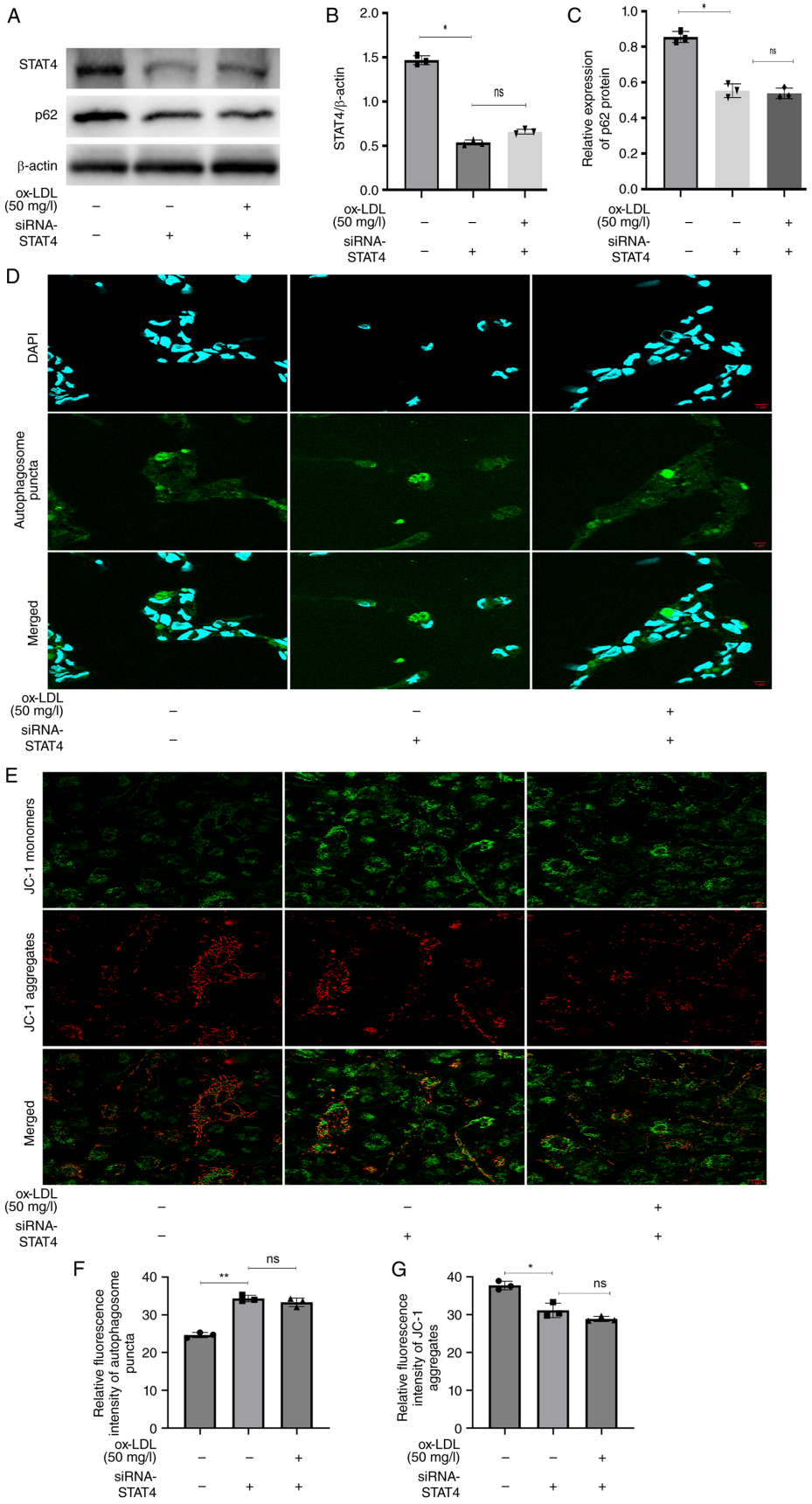

Figure 6. STAT4 silencing prevents ox-LDL-induced impairment of autophagic flux and mitochondrial dysfunction. (A) Western blot analysis of (B) STAT4 and (C) p62 in STAT4-silencing THP-1 cells treated with ox-LDL and BHB. (D) Confocal microscopy image of autophagosome puncta in siRNA-STAT4 THP-1 cells after treatment. Nuclei were visualized by counterstaining with DAPI (magnification, x60). (E) JC-1 staining of THP-1 cells visualized by fluorescence confocal microscopy. Fluorescence was recorded using 488 nm excitation (magnification, x60). Relative fluorescence intensity of (F) autophagosome puncta and (G) JC-1 aggregates in siRNA-STAT4 THP-1 cells after treatment. The group without 50 mg/l ox-LDL and siRNA-STAT4 treatment was transfected with negative control siRNA. *P<0.05, **P<0.01. ox-LDL, oxidized low-density lipoprotein; BHB, β-hydroxybutyrate; si/siRNA, small interfering; ns, not significant.

inhibition, facilitating the clearance of ox-lipids (44). In BHB-treated macrophages, the suppression of STAT1 coupled with the activation of STAT6 preserves mitochondrial integrity and promotes autophagy-mediated cholesterol efflux, thereby decreasing foam cell transformation (54). This crosstalk highlights STATs as a link between metabolic reprogramming and cell quality control.

Mitochondrial dysfunction is increasingly recognized as a central driver of vascular injury (55,56). The NADH dehydrogenase (ubiquinone) Fe-S protein 4 (NDUFS4)-sirtuin 5 (SIRT5)-dual specificity phosphatase 1 (DUSP1) axis regulates mitochondrial unfolded protein response (mtUPR) and energy metabolism, thereby protecting against coronary microvascular injury during ischemia-reperfusion (57). Similarly, targeting the SIRT5/DUSP1 pathway is a promising strategy for mitochondrial repair in doxorubicin-induced cardiotoxicity (58). In the present study, BHB restored autophagic activity and $\Delta\Psi m$, which may involve analogous pathways, as STAT4 modulation may intersect with these mitochondrial regulatory networks.

The interplay between mitochondria and the endoplasmic reticulum (ER) has emerged as a key determinant of cell stress responses (59). Astragaloside IV attenuates mechanical stress-induced cardiac remodeling through the Piezo1-voltage-dependent anion channel 1 axis, which regulates ER UPR (60). Tanshinone IIA modulates METTL3- and SIRT5-mediated UPR pathways to govern mitochondria-ER crosstalk in coronary microvascular injury (61). The potential involvement of ER-mitochondria coupling in ox-LDL-challenged macrophages warrants further investigation.

Mitophagy and mitochondrial dynamics are key nodes in mitochondrial quality control networks. The nuclear receptor subfamily 4 group A member 1-mitochondrial fission factor-FUN14 domain containing 1 axis regulates mitochondrial fragmentation and mitophagy in myocardial ischemia-reperfusion injury (62). In atherosclerosis, targeting of the transmembrane BAX inhibitor motif containing 6/NDUFS4 pathway restores mitophagy and suppresses necroptosis (63). The present study demonstrated that BHB enhancement autophagic function may extend to mitophagy regulation, potentially via STAT4-dependent mechanisms. In addition, the DNA-dependent protein kinase catalytic subunit-yes-associated protein 1-ferroptosis axis is implicated in diabetic cardiomyopathy (64), suggesting broader crosstalk between DNA damage responses and organelle homeostasis.

The present study had certain limitations that warrant consideration. A key limitation of this study is the assessment of autophagy primarily through steady-state levels of LC3-II and p62 without the use of lysosomal inhibitors to directly measure autophagic flux. Future investigations should establish the dynamics of the autophagic process and include standard pharmacological approaches using bafilomycin A1 or chloroquine to trace LC3-II and p62 turnover. The present study used monodansylcadaverine-based staining, which does not distinguish between autophagosomes and autolysosomes and does not give a definitive assessment of autophagic flux. Furthermore, employing more advanced techniques such as live-cell imaging with tandem fluorescent-tagged LC3 [red fluorescent protein (RFP)-green fluorescent protein (GFP)-LC3] is required to confirm whether the present changes represent an upregulation of functional autophagy or a potential impairment at the fusion/degradation stage. This method allows precise discrimination between autophagosomes (GFP^+/RFP+) and autolysosomes (GFP-/RFP+), providing a direct and quantitative measure of autophagic flux and maturation independently of lysosomal inhibitors (65). The present findings were derived from *in vitro* experiments using THP-1 macrophage cell lines, which may not fully replicate the complex physiological and pathological contexts of human atherosclerosis. The modulation of STAT4 underscores the complexity of the signaling pathways involved. Specifically, the present data do not demonstrate whether STAT4 acts upstream or downstream of mitochondrial functional changes. To identify the mechanistic interplay between STAT4 signaling and autophagy, subsequent experiments should assess levels of phosphorylated STAT4 and STAT4 nuclear localization to validate the activation status and subcellular distribution of STAT4 in response to BHB.

In conclusion, the present study demonstrated the detrimental effects of ox-LDL on autophagic flux and mitochondrial function in THP-1 macrophages, while highlighting the potential of BHB to restore these processes. The present findings contribute to understanding of the cell mechanisms underlying lipid metabolism and inflammation and suggest BHB may be a promising therapeutic candidate for the treatment of atherosclerosis. Future studies should investigate the translational potential of these findings *in vivo* to validate the clinical applicability of BHB in cardiomyocyte energy metabolism and CVD.

Acknowledgements

Not applicable.

Funding

The present study was supported by the Joint Construction Project of the Henan Provincial Medical Science and Technology Research Program (grant no. LHGJ20230035), Henan Natural Science Foundation (grant no. 222300420355) from the Henan Provincial Department of Education and the Henan Province Science and Technology Research Program Project (grant no. SBGJ202103016) from the Henan Provincial Health Commission.

Availability of data and materials

The data generated in the present study may be requested from the corresponding author.

Authors' contributions

WL designed the study and wrote the manuscript. MH performed the experiments. WL and HW analyzed the data. WL and HW confirm the authenticity of all the raw data. All authors read and approved the final manuscript.

Ethics approval and consent to participate

Not applicable.

Patient consent for publication

Not applicable.

Competing interests

The authors declare that they have no competing interests.

References

1. Roth GA, Mensah GA, Johnson CO, Addolorato G, Ammirati E, Baddour LM, Barengo NC, Beaton AZ, Benjamin EJ, Benziger CP, *et al*: Global burden of cardiovascular diseases and risk factors, 1990-2019: Update from the GBD 2019 study. J Am Coll Cardiol 76: 2982-3021, 2020.
2. Zhi X, Sun Y, Cai F, Wang S, Gao H, Wu F, Zhang L and Shen Z: Oxidized Low-density lipoprotein (Ox-LDL)-triggered double-lock probe for spatiotemporal lipoprotein oxidation and atherosclerotic plaque imaging. Adv Healthc Mater 12: e2301595, 2023.
3. Qiao YN, Zou YL and Guo SD: Low-density lipoprotein particles in atherosclerosis. Front Physiol 13: 931931, 2022.
4. Obermayer G, Afonyushkin T and Binder CJ: Oxidized low-density lipoprotein in inflammation-driven thrombosis. J Thromb Haemost 16: 418-428, 2018.
5. Thangasparan S, Kamisah Y, Ugusman A, Mohamad Anuar NN and Ibrahim N: Unravelling the Mechanisms of oxidised Low-density lipoprotein in cardiovascular health: Current evidence from in vitro and in vivo studies. Int J Mol Sci 25: 13292, 2024.
6. Munno M, Mallia A, Greco A, Modafferi G, Banfi C and Eligini S: Radical oxygen species, oxidized low-density lipoproteins, and lectin-like oxidized low-density lipoprotein receptor 1: A vicious circle in atherosclerotic process. Antioxidants (Basel) 13: 583, 2024.
7. He Y and Liu T: Oxidized low-density lipoprotein regulates macrophage polarization in atherosclerosis. Int Immunopharmacol 120: 110338, 2023.
8. Huang L and Guo H: Acetylation modification in the regulation of macroautophagy. Adv Biotechnol (Singap) 2: 19, 2024.
9. Zhang X, Misra SK, Moitra P, Zhang X, Jeong SJ, Stitham J, Rodriguez-Velez A, Park A, Yeh YS, Gillanders WE, *et al*: Use of acidic nanoparticles to rescue macrophage lysosomal dysfunction in atherosclerosis. Autophagy 19: 886-903, 2023.
10. Li P, Li H, Li X, Li S, Xu H, Cui J, Cheng G, Liu Y, Xu X, Xin Y and Liu A: San Jie tong Mai fang protects against atherosclerosis progression by regulating macroautophagy through the PI3K/AKT/mTOR signaling pathway. J Cardiovasc Pharmacol 82: 333-343, 2023.
11. Salminen A and Kaarniranta K: Regulation of the aging process by autophagy. Trends Mol Med 15: 217-224, 2009.
12. Robichaud S, Fairman G, Vijithakumar V, Mak E, Cook DP, Pelletier AR, Huard S, Vanderhyden BC, Figeys D, Lavallée-Adam M, *et al*: Identification of novel lipid droplet factors that regulate lipophagy and cholesterol efflux in macrophage foam cells. Autophagy 17: 3671-389, 2021.
13. Seidenberg J, Stellato M, Hukara A, Ludewig B, Klingel K, Distler O, Błyszczuk P and Kania G: The AP-1 transcription factor Fosl-2 regulates autophagy in cardiac fibroblasts during myocardial fibrogenesis. Int J Mol Sci 22: 1861, 2021.
14. Wu Y, Teng Y, Zhang C, Pan Y, Zhang Q, Zhu X, Liu N, Su X and Lin J: The ketone body β-hydroxybutyrate alleviates CoCrMo alloy particles induced osteolysis by regulating NLRP3 inflammasome and osteoclast differentiation. J Nanobiotechnology 20: 120, 2022.
15. Chu Y, Hua Y, He L, He J, Chen Y, Yang J, Mahmoud I, Zeng F, Zeng X, Benavides GA, *et al*: beta-hydroxybutyrate administered at reperfusion reduces infarct size and preserves cardiac function by improving mitochondrial function through autophagy in male mice. J Mol Cell Cardiol 186: 31-44, 2024.
16. Liu Y, Wang W, Zhang J, Gao S, Xu T and Yin Y: JAK/STAT signaling in diabetic kidney disease. Front Cell Dev Biol 11: 1233259, 2023.
17. Billah M, Ridiandries A, Allahwala UK, Mudaliar H, Dona A, Hunyor S, Khachigian LM and Bhindi R: Remote ischemic preconditioning induces cardioprotective autophagy and signals through the IL-6-Dependent JAK-STAT pathway. Int J Mol Sci 21: 1692, 2020.
18. Chen D, Liu Y, Chen J, Lin H, Guo H, Wu Y, Xu Y, Zhou Y, Zhou W, Lu R, *et al*: JAK/STAT pathway promotes the progression of diabetic kidney disease via autophagy in podocytes. Eur J Pharmacol 902: 174121, 2021.
19. Liu Z, Hu K, Chen YS, Huang YJ, Hu Q, Zeng W, Cao Y, Xiao Q and Zhang XK: JAK2/STAT3 inhibition attenuates intestinal ischemia-reperfusion injury via promoting autophagy: In vitro and in vivo study. Mol Biol Rep 49: 2857-2867, 2022.
20. Zhang Y, Liu M, Wu Y, Xu Y, Hong Y and Xiang H: Insulin-like growth factor 1 knockdown attenuates high glucose-induced podocyte injury by promoting the JAK2/STAT signalling-mediated autophagy. Nephrology (Carlton) 29: 394-404, 2024.
21. Madhavan A, Arun KB, Pushparajan AR, Balaji M and Kumar RA: Transcription repressor protein ZBTB25 associates with HDAC1-Sin3a complex in *Mycobacterium tuberculosis*-infected macrophages, and its inhibition clears pathogen by autophagy. mSphere 6: e00036-21, 2021.
22. Gao Y, Chen S, Jiao S, Fan Y, Li X, Tan N, Fang J, Xu L, Huang Y, Zhao J, *et al*: ATG5-regulated CCL2/MCP-1 production in myeloid cells selectively modulates anti-malarial CD4+ Th1 responses. Autophagy 20: 1398-1417, 2024.
23. Scarno G, Mazej J, Laffranchi M, Di Censo C, Mattiola I, Candelotti AM, Pietropaolo G, Stabile H, Fionda C, Peruzzi G, *et al*: Divergent roles for STAT4 in shaping differentiation of cytotoxic ILC1 and NK cells during gut inflammation. Proc Natl Acad Sci USA 120: e2306761120, 2023.
24. Zhang X, Wang Y and Lv J: STAT4 targets KISS1 to inhibit the oxidative damage, inflammation and neuronal apoptosis in experimental PD models by inactivating the MAPK pathway. Neurochem Int 175: 105683, 2024.
25. Livak KJ and Schmittgen TD: Analysis of relative gene expression data using real-time quantitative PCR and the 2(-Delta Delta C(T)) method. Methods 25: 402-408, 2001.
26. Semenova N, Yakisich JS, Ascue R, Iyer AKV and Azad N: Reversible upregulation of the Senescence-Associated Beta-Galactosidase marker induced by cell detachment in cancer cells. Cells 14: 1667, 2025.
27. Sanchez-Leon ME, Loaeza-Reyes KJ, Matias-Cervantes CA, Mayoral-Andrade G, Pérez-Campos EL, Pérez-Campos-Mayoral L, Hernández-Huerta MT, Zenteno E, Pérez-Cervera Y and Pina-Canseco S: LOX-1 in cardiovascular disease: A comprehensive molecular and clinical review. Int J Mol Sci 25: 5276, 2024.
28. Kishimoto H, Akagi M, Zushi S, Teramura T, Onodera Y, Sawamura T and Hamanishi C: Induction of hypertrophic chondrocyte-like phenotypes by oxidized LDL in cultured bovine articular chondrocytes through increase in oxidative stress. Osteoarthritis Cartilage 18: 1284-1290, 2010.
29. Palmer AK, Spinelli R, Prata LGL, Chaib S, Suda M, Tchkonia T, Smith U and Kirkland JL: Senotherapeutics for metabolic disease and diabetic complications. J Intern Med 299: 2-19, 2026.
30. Hao T, Fang W, Xu D, Chen Q, Liu Q, Cui K, Cao X, Li Y, Mai K and Ai Q: Phosphatidylethanolamine alleviates OX-LDL-induced macrophage inflammation by upregulating autophagy and inhibiting NLRP1 inflammasome activation. Free Radic Biol Med 208: 402-417, 2023.
31. Wang G, Chen JH, Qiang Y, Wang DZ and Chen Z: Decreased STAT4 indicates poor prognosis and enhanced cell proliferation in hepatocellular carcinoma. World J Gastroenterol 21: 3983-3993, 2015.
32. Miao X, Pan R and Chang F: Down-regulation of ATP8B2 in foam cells inhibits autophagic flux and ox-LDL degradation in atherosclerosis. Cell Biochem Biophys 83: 3451-3463, 2025.
33. Yang J, Ma X, Niu D, Sun Y, Chai X, Deng Y, Wang J and Dong J: PCSK9 inhibitors suppress oxidative stress and inflammation in atherosclerotic development by promoting macrophage autophagy. Am J Transl Res 15: 5129-5144, 2023.
34. Gu HF, Li HZ, Tang YL, Tang XQ, Zheng XL and Liao DF: Nicotinate-Curcumin impedes foam cell formation from THP-1 cells through restoring autophagy flux. PLoS One 11: e0154820, 2016.
35. Zhou P, Zhang Q, Yang Y, Wu W, Chen D, Zheng Z, Jongkaewwattana A, Jin H, Zhou H and Luo R: Cleavage of SQSTM1/p62 by the Zika virus protease NS2B3 prevents autophagic degradation of viral NS3 and NS5 proteins. Autophagy 20: 2769-2784, 2024.
36. Wu K, Seylani A, Wu J, Wu X, Bleck CKE and Sack MN: BLOC1S1/GCN5L1/BORCS1 is a critical mediator for the initiation of autolysosomal tubulation. Autophagy 17: 3707-3724, 2021.

37. Zhan Q, Jeon J, Li Y, Huang Y, Xiong J, Wang Q, Xu TL, Li Y, Ji FH, Du G and Zhu MX: CAMK2/CaMKII activates MLKL in short-term starvation to facilitate autophagic flux. Autophagy 18: 726-744, 2022.
38. Yuan X, Tian GG, Pei X, Hu X and Wu J: Spermidine induces cytoprotective autophagy of female germline stem cells in vitro and ameliorates aging caused by oxidative stress through upregulated sequestosome-1/p62 expression. Cell Biosci 11: 107, 2021.
39. Cui X, Wang B, Han D, Cheng M, Yuan P, Du P, Hou Y, Su C, Tang J and Zhang J: Exacerbation of atherosclerosis by STX17 knockdown: Unravelling the role of autophagy and inflammation. J Cell Mol Med 28: e18402, 2024.
40. Yuan L, Fan L, Zhang Z, Huang X, Liu Q and Zhang Z: Procyanidin B2 alleviates oxidized low-density lipoprotein-induced cell injury, inflammation, monocyte chemotaxis, and oxidative stress by inhibiting the nuclear factor kappa-B pathway in human umbilical vein endothelial cells. BMC Cardiovasc Disord 24: 231, 2024.
41. Hua J, Gao Z, Zhong S, Wei B, Zhu J and Ying R: CISD1 protects against atherosclerosis by suppressing lipid accumulation and inflammation via mediating Drp1. Biochem Biophys Res Commun 577: 80-88, 2021.
42. Wang Z, Wang L, Wang Y and Zhang J: Erianin protects human umbilical vein endothelial cells from oxidized Low-Density Lipoprotein-Induced apoptosis and oxidative stress through activation of nuclear factor E2-Related factor 2 signaling. Chem Biol Drug Des 105: e70104, 2025.
43. Bai YP, Xing YJ, Ma T, Li K, Zhang T, Wang DG, Wan SJ, Zhang CW, Sun Y and Wang MY: beta-Hydroxybutyrate suppresses M1 macrophage polarization through beta-hydroxybutyrylation of the STAT1 protein. Cell Death Dis 15: 874, 2024.
44. Huang C, Wang J, Liu H, Huang R, Yan X, Song M, Tan G and Zhi F: Ketone body β-hydroxybutyrate ameliorates colitis by promoting M2 macrophage polarization through the STAT6-dependent signaling pathway. BMC Med 20: 148, 2022.
45. Zhang N, Liu C, Jin L, Zhang R, Wang T, Wang Q, Chen J, Yang F, Siebert HC and Zheng X: Ketogenic diet elicits antitumor properties through inducing oxidative stress, inhibiting MMP-9 expression, and rebalancing M1/M2 Tumor-associated macrophage phenotype in a mouse model of colon cancer. J Agric Food Chem 68: 11182-11196, 2020.
46. Xu Z, Zhang M, Li X, Wang Y and Du R: Exercise ameliorates atherosclerosis via Up-regulating serum β-Hydroxybutyrate levels. Int J Mol Sci 23: 3788, 2022.
47. Ehtiati S, Hatami B, Khatami SH, Tajernarenj K, Abdi S, Sirati-Sabet M, Ghazizadeh Hashemi SAH, Ahmadzade R, Hamed N, Goudarzi M, *et al*: The multifaceted influence of Beta-Hydroxybutyrate on autophagy, mitochondrial metabolism, and epigenetic regulation. J Cell Biochem 126: e70050, 2025.
48. Ji LW, Deng Y and Li T: Effect of Ketone Body β-Hydroxybutyrate to attenuate inflammation-induced mitochondrial oxidative stress in vascular endothelial cells. Sichuan Da Xue Xue Bao Yi Xue Ban 52: 954-959, 2021 (In Chinese).
49. Huang X, Xie M, Wang Y, Lu X, Mei F, Zhang K, Yang X, Chen G, Yin Y, Feng G, *et al*: Porphyromonas gingivalis aggravates atherosclerotic plaque instability by promoting lipid-laden macrophage necroptosis. Signal Transduct Target Ther 10: 171, 2025.
50. Cui Y, Chen Y, Li H, Zhang W, Wang X, Xia M, Gan N, Zhou Y, Li M, Zhang H, *et al*: PCSK9 Promotes Atherosclerotic Plaque Instability by Inducing VSMC Ferroptosis through the YAP1-NUPR1 Axis. Research (Wash D C) 8: 0922, 2025.
51. Hu W, Liu H, Lin L, Li M, Fan Z, Zhang Y, Lin X and Qi Y: Feedback inhibition of the Janus kinase/signal transducer and activator of transcription signaling pathway by CG5953 through Ptp61F. Int J Biol Macromol 330: 147875, 2025.
52. Ji L, He Q, Liu Y, Deng Y, Xie M, Luo K, Cai X, Zuo Y, Wu W, Li Q, *et al*: Ketone Body β-hydroxybutyrate prevents myocardial oxidative stress in septic cardiomyopathy. Oxid Med Cell Longev 2022: 2513837, 2022.
53. Lu F, Wang R, Cheng Y and Li X: Preconditioning with β-hydroxybutyrate attenuates lung ischemia-reperfusion injury by suppressing alveolar macrophage pyroptosis through the SIRT1-FOXO3 signaling pathway. FASEB J 38: e70027, 2024.
54. Wang C, Xu W, Jiang S, Wu Y, Shu J, Gao X and Huang K: β-Hydroxybutyrate facilitates postinfarction cardiac repair via targeting PHD2. Circ Res 136: 704-718, 2025.
55. Marcheggiani F, Nunzi I, Rao L, Dhaouadi N, Nesci S, Pinton P and Marchi S: Mitochondrial dysfunction in cerebrovascular diseases. Trends Mol Med: Apr 30, 2026 doi: 10.1016/j.molmed.2026.04.002 (Epub ahead of print).
56. Yang W, He J, Yu H, Wu Y and Shi S: Mitochondrial dysfunction: Potential therapy for abdominal aortic aneurysms. Curr Vasc Pharmacol 23: 255-271, 2025.
57. Pu X, Liu J, Wang Y, Guan X, Wu Q, Zhang Q, Liu R and Chang X: Ginsenoside Rb1 attenuates coronary microvascular inflammatory injury via NDUFS4-SIRT5-DUSP1-mediated mitochondrial quality control in a murine ischemia-reperfusion model. J Ginseng Res 49: 509-522, 2025.
58. Shi H, Pang B, Zhang F, Guo Z, Xu W, Zheng M, You Y, Liu G, Nie Y, Liang J and Chang X: A novel ligustrazine-based nanodelivery system protects against doxorubicin-induced cardiotoxicity by targeting the SIRT5-DUSP1 axis for mitochondrial repair. J Nanobiotechnology 23: 681, 2025.
59. Padhy B, Xie J, Idrees D, Cheng CJ and Huang CL: Endoplasmic reticulum-mitochondrion disconnection promotes metabolic reprogramming and cystogenesis in polycystic kidney disease. bioRxiv: Nov 12, 2025 (Epub ahead of print). doi: 10.1101/2025.10.31.685870.
60. Zhang S, Gao W, Gao X, Xu W, Liu Y, Guo Z, Liu G, Zhang P, Shi H and Chang X: Astragaloside VI attenuates mechanical stress-induced cardiac remodeling through piezo1-VDAC1 dependent endoplasmic reticulum unfolded protein response. Phytomedicine 148: 157288, 2025.
61. Pu X, Wu Q, Yan Z, Zhou S, Zhang Q, Zhang X, Cai Y, Liu Z, Liu R and Chang X: Tanshinone IIA modulates Sirt5 and Metll3 interaction to govern mitochondria-endoplasmic reticulum unfolded protein response in coronary microvascular injury. Phytomedicine 145: 156982, 2025.
62. Wang J, Zhuang H, Jia L, He X, Zheng S, Ji K, Xie K, Ying T, Zhang Y, Li C and Chang X: Nuclear receptor subfamily 4 group A member 1 promotes myocardial ischemia/reperfusion injury through inducing mitochondrial fission factor-mediated mitochondrial fragmentation and inhibiting FUN14 domain containing 1-depedent mitophagy. Int J Biol Sci 20: 4458-4475, 2024.
63. Chang X, Zhou H, Hu J, Ge T, He K, Chen Y, Zou R and Fan X: Targeting mitochondria by lipid-selenium conjugate drug results in malate/fumarate exhaustion and induces mitophagy-mediated necroptosis suppression. Int J Biol Sci 20: 5793-5811, 2024.
64. Wang J, Chang X, Li C, Gao J, Guo Z, Zhuang H, Wang L, Huang Y, Wang W, Li C and He Q: DNA-PKcs-Driven YAP1 phosphorylation and nuclear translocation: A key regulator of ferroptosis in hyperglycemia-induced cardiac dysfunction in type 1 diabetes. Adv Sci (Weinh) 12: e2412698, 2025.
65. Jiang XL, Liu B, Li JK, Lin YF, Zhu PL, Zhang Z, Wang Y, Deng B, Zhang JZ and Yung KK: Przewaquinone A, as a natural STAT3 inhibitor, suppresses the growth of melanoma cells and induces autophagy. Phytomedicine 142: 156810, 2025.